

Journal of Materials Chemistry A

Accepted Manuscript



This is an *Accepted Manuscript*, which has been through the Royal Society of Chemistry peer review process and has been accepted for publication.

Accepted Manuscripts are published online shortly after acceptance, before technical editing, formatting and proof reading. Using this free service, authors can make their results available to the community, in citable form, before we publish the edited article. We will replace this *Accepted Manuscript* with the edited and formatted *Advance Article* as soon as it is available.

You can find more information about *Accepted Manuscripts* in the [Information for Authors](#).

Please note that technical editing may introduce minor changes to the text and/or graphics, which may alter content. The journal's standard [Terms & Conditions](#) and the [Ethical guidelines](#) still apply. In no event shall the Royal Society of Chemistry be held responsible for any errors or omissions in this *Accepted Manuscript* or any consequences arising from the use of any information it contains.

Cite this: DOI: 10.1039/c0xx00000x

PAPER

www.rsc.org/xxxxxx

A Bulky and Flexible Electrocatalyst for Efficient Hydrogen Evolution based on the Growth of MoS₂ Nanoparticles on Carbon Nanofibers Foam

Xin Guo,^{&,a} Guo-lin Cao,^{&,a} Fei Ding,^b Xinyuan Li,^a Shuyu Zhen^a, Yi-fei Xue,^a Yi-ming Yan^{* a},
Ting Liu^{* a}, and Ke-ning Sun^{* a}

Received (in XXX, XXX) Xth XXXXXXXXX 20XX, Accepted Xth XXXXXXXXX 20XX

DOI: 10.1039/b000000x

An advanced hydrogen evolution reaction (HER) electrocatalyst is highly desired for development of solar water-splitting devices. In this work, we describe the preparation of flexible, three-dimensional and durable electrode, which composed of MoS₂ nanoparticles grown on bacteria-cellulose-derived carbon fibers foam (MoS₂/CNFs). The MoS₂/CNFs foam was used as a bulky and flexible HER electrocatalyst, exhibiting excellent catalytic activity for a hydrogen evolution reaction in an acidic electrolyte (16 mA cm⁻² at an overpotential of 230 mV). Remarkably, this novel HER electrocatalyst shows a low onset overpotential of 120 mV, a small Tafel slope of 44 mV dec⁻¹, a high exchange current density of 0.09 mA cm⁻², and a Faradaic efficiency of nearly 100 %. This work offers an attractive strategy of preparing bulky and flexible electrocatalyst for large-scale water splitting technology.

1. Introduction

Hydrogen (H₂), as an efficient energy carrier and clean energy resource, has been vigorously pursued to resolve the global issues of severe energy shortage and environmental deterioration.¹⁻² In particular, sustainable hydrogen production with water splitting technology by using renewable energy in the form of electricity is considered as a practical way. However, an advanced HER electrocatalyst is the central to the development of effective water splitting technology. Recently, Mo-based compounds have been intensively investigated as cheap, robust and highly efficient HER electrocatalysts, aiming to replace the noble metals based electrocatalysts, such as platinum and its alloys.³ To this end, several examples including MoS₂,⁴⁻⁸ MoSe₂,⁹⁻¹⁰ Mo₂C,¹¹⁻¹² MoB,¹³ NiMoN_x/C,¹⁴ Co_{0.6}Mo_{1.4}N₂¹⁵ were well-reported as suitable HER electrocatalysts.

Among different Mo-based HER electrocatalysts, Molybdenum disulfide (MoS₂) has attracted extremely much interest due to its unique structural and remarkably catalytic properties. Both computational and experimental studies have demonstrated that the high HER activity of MoS₂ originates from the sulfur edges, while the basal planes are inert.¹⁶⁻¹⁷ Nevertheless, the HER performance of MoS₂ is largely limited by its poor conductivity and serious aggregation of the resulted samples. To resolve these problems, nanosized MoS₂, supposed to expose much more sulfur edge sites, were confined into a conductive templates or supports to improve the catalytic activity of the host

material. Several efforts have been made to enhance the HER performance of MoS₂ by incorporating MoS₂ with graphene,¹⁸⁻²⁰ carbon nanotube (CNTs),²¹ and other mesoporous carbon²² to form MoS_x-based hybrid or composite. Dai et. al.²³ reported the synthesis of MoS₂ on reduced graphene oxide sheets and obtained high HER performance of the resulting hybrid, while Yang and coworkers²⁴ confined MoS₂ nanosheets into graphite, producing a size-controlled MoS₂/RGO composites for HER catalysis. More recently, chemical vapor deposition (CVD) method was used to grow MoS₂ nanocrystals on the electrospinning derived carbon nanofibers, resulting a 3D rose-petal-shaped HER catalyst.²⁵ These works indicate that rational designed structure preferentially exposed more catalytically active edge sites can improve HER performance.

Despite these achievements, it is highly desirable to design and synthesize a highly efficient MoS₂-carbon based HER electrocatalyst by taking into account the following important factors: 1) HER involves a gas evolution process at the surface of electrocatalyst. Thus, a 3D porous structure of the electrocatalyst should benefit for high catalytic performance either owing to high catalyst loadings, or due to a facilitated reaction kinetic in the channel-rich structure. 2) Dense and intimate contacting of MoS₂ with carbon substrate should be essentially required to achieve high MoS₂ loading and good electrical conductivity, therefore improving the HER performance. 3) In contrast to traditional powder catalyst, a flexible and bulky electrocatalyst with high mechanical stiffness, chemical stability and electrical properties

are superior to be used as binder-free electrode for HER. Keep these goals in mind, in this work, we present our recent efforts in developing a 3D, binder-free foam electrode for HER.

Bacterial cellulose (BC), a bio-product produced from fermentation, has been widely used to prepare carbon nanofibers.²⁶ To date, the CNFs aerogel have been used to prepare 3D electrode materials for supercapacitors,²⁷⁻²⁸ catalyst supports²⁹ and lithium-ion batteries.³⁰ The major advantages of using BC include easy fabrication, low cost and its mechanically robust 3D network structures, which is a key point for the electrochemical performance of the final composites. Here, we fabricate CNFs foam with a modified synthetic method and consequently incorporate the nanosized MoS₂ into the CNFs foam, resulting a bulky and flexible, binder-free HER electrocatalyst. Remarkably, the obtained MoS₂/CNFs exhibits a low onset overpotential of 120 mV, a small Tafel slope of 44 mV dec⁻¹, and a high exchange current density of 0.09 mA cm⁻². Moreover, an extremely low overpotential of 230 mV was needed to drive current densities of 16 mA cm⁻². This novel HER catalyst maintains its activity for at least 16 hours under acidic conditions with a Faradaic efficiency (FE) of nearly 100 %.

2. Experimental Section

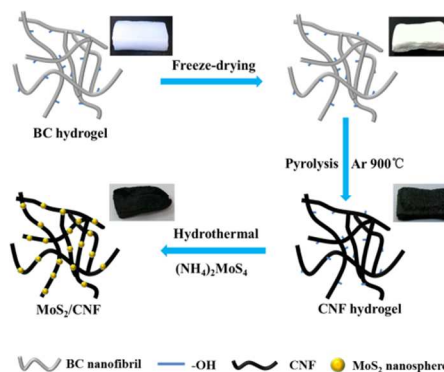
Synthesis of MoS₂/CNFs. CNF aerogel were fabricated by a direct pyrolysis of the BC aerogel obtained from freeze-dried BC hydrogel under flowing Argon (Ar) atmosphere at 900 °C for 2 hours. Then, 22 mg of (NH₄)₂MoS₄ was added to 10 mg of CNF aerogel immersed in 10 mL of DMF. The mixture was sonicated at room temperature for approximately 10 min until a clear and homogeneous solution was achieved. After that, 0.1 mL of N₂H₄·H₂O was added. The solution was further sonicated for 30 min before transferred to a 40 mL Teflon-lined autoclave, and then was heated in an oven at 200 °C for 10 h with no intentional control of ramping or cooling rate. Product was collected by centrifugation at 4500 rpm for 5 min, and then washed with deionized (DI) water. The washing step was repeated for at least 5 times to ensure that most DMF was removed. Finally, the product was dispersed in 5 mL of DI water, frozen by liquid nitrogen and lyophilized overnight. The obtained bulky material was referred as MoS₂/CNFs. The preparation process of bare MoS₂ and the CNFs connected MoS₂ particles was similar to that described above, but without adding CNFs and replacing the DMF with water.

The morphology of samples was characterized by the scanning electron microscope (SEM, QUANTA FEG 250) and high resolution transmission electron microscope (HRTEM, JEOL JEM 2010). The obtained products were characterized by X-ray diffraction (XRD, RigakuUltima IV, Cu K α radiation, 40 KV, 40 mA). X-ray photoelectron spectroscopy (XPS) was carried out on Physical Electronics 5400 ESCA.

The working electrodes were fabricated by cutting a piece of the MoS₂/CNFs (1.5 × 1 × 0.1 cm³) and the edge of one side was glued with silver wire using silver paste. Electrochemical measurements were performed in a three-electrode glass cell on a CHI 760 D (Shanghai Chenhua Instrument) using above MoS₂/CNFs foam as working electrodes, Pt wire as a counter electrode and saturated calomel electrode as a reference electrode. Linear sweep voltammetry with scan rate of 2 mV s⁻¹ was

conducted in 0.5 M H₂SO₄. In all experiments, the electrolyte solutions were purged with N₂ for 15 min prior to the experiments in order to remove oxygen. During the measurements, the electrochemical cell was kept under N₂ atmosphere. All the potentials reported in our manuscript were referenced to a reversible hydrogen electrode (RHE) by unified with a value of (0.241+0.059 pH) V.

3. Results and Discussion



Scheme 1. Synthesis procedure of the MoS₂/CNFs electrocatalyst.

The synthesis of MoS₂/CNFs foam is illustrated in Scheme 1. BC hydrogel was freeze-dried to remove the water while maintaining its porous nanostructure. Subsequently, the CNFs hydrogel was fabricated by directly pyrolyzing the freeze-dried BC hydrogel under flowing Ar atmosphere at 900 °C for 2 h. Finally, MoS₂/CNFs foam was obtained by a simple one-step solvothermal reaction of (NH₄)₂MoS₄ and hydrazine in an N, N-dimethylformamide (DMF) solution immersed with CNFs foam. During this process, the MoS₂ was in-situ decorated into the CNFs framework. As seen, the obtained CNFs foam was black, while the growth of MoS₂ on CNFs does not obviously change the color and shape of the sample.

Figure 1 shows scanning electron microscopy (SEM) images of the bare MoS₂, BC hydrogel, CNFs hydrogel and MoS₂/CNFs foam. The SEM of bare MoS₂ sample shows aggregated particles with random size (Figure 1a). The BC hydrogel displays a porous structure with interconnected nanowires (Figure 1b). Figure 1c shows that, after pyrolysis, the generated CNFs foam maintains perfectly the structure of BC hydrogel. The diameter of the carbonized nanowires in CNFs foam was estimated to be 20-30 nm. After the growth of MoS₂, as shown in Figure 1d, the resulting MoS₂/CNFs exhibits that the CNFs nanowires were clearly decorated with MoS₂ nanoparticles. Notably, the size of the MoS₂ nanoparticles in CNFs foam were greatly decreased comparing to the bare MoS₂. It suggests that the CNFs framework might suppress the aggregation of MoS₂ particles during the synthesis.

Figure 2a shows the transmission electron microscopy (TEM) image of the bare MoS₂, revealing that it was consisted of more refined nanoparticles with a size of 8 ± 2 nm. Such uniformly distributed MoS₂ nanoparticles with small size are expected to expose more active sites for HER. The morphology of the as-prepared MoS₂/CNFs is shown in Figure 2b. As seen, numerous

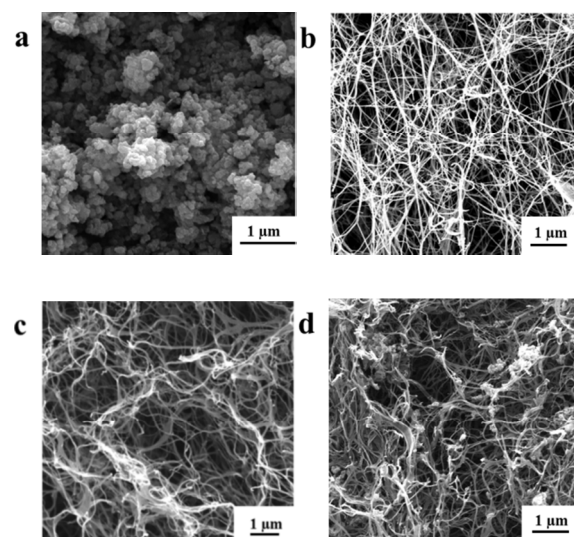


Figure 1. SEM images of (a) bare MoS₂, (b) BC hydrogel, (c) CNF hydrogel and (d) MoS₂/CNFs hybrid.

5

MoS₂ nanoparticles are uniformly decorated on the CNFs. A further close observation by TEM indicates that the MoS₂ nanoparticles were intimately grown on the surface of the skeleton of CNFs (Figure 2c). The grown MoS₂ nanoparticles were further characterized by high resolution TEM (HRTEM) image. Figure 2d is the HRTEM image of the white ellipse in (c), which shows the MoS₂ nanoparticles are amorphous in the MoS₂/CNFs hybrid.

The solvent of DMF plays important role in determining the morphology and structure of the prepared MoS₂/CNFs. For comparison, we conducted a control experiment by replacing DMF with water as the solvent. As a result, only a simple mixture of MoS₂ nanoparticles and CNFs was obtained (Figure S1). In the resulted hybrid, CNFs only serves as nanowires holding for the aggregated MoS₂ particles. Moreover, we have tested the HER activity of MoS₂/CNFs hybrid by replacing the DMF with water

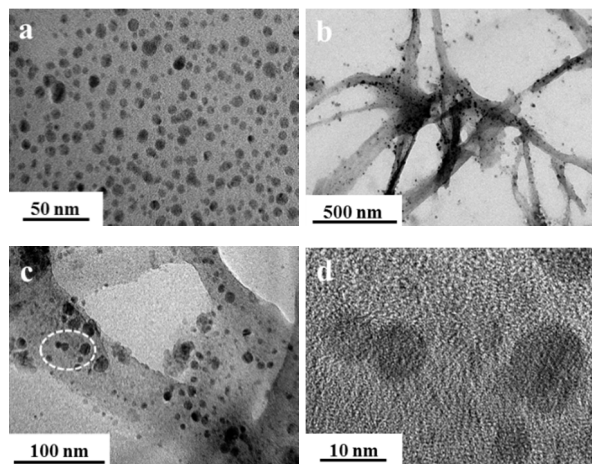


Figure 2. TEM images of (a) MoS₂ nanoparticles and (b and c) MoS₂/CNFs. (d) HRTEM image of the white ellipse in (c).

as solvent. As shown in the Figure S2, this sample exhibits much poorer performance than the as-prepared MoS₂/CNFs hybrid. Such a huge morphological difference highlights the importance of DMF as a solvent for mediating the formation and dispersion

of MoS₂ nanoparticles, which contributes to the prominent performance for the HER. To further gain the structural information of the samples, X-ray diffraction (XRD) and Raman spectroscopy were performed. Figure S3 (a) shows that no sharp peaks were observed for the pure MoS₂ nanoparticles, indicating poorly crystallized structure of the solvothermally synthesized MoS₂ before annealing treatment. The observed three broad and weak diffraction peaks centered at around 2θ of 15.0°, 33.8°, and 57.1° should be assigned to (002), (100), and (110) planes of the hexagonal MoS₂ (2H-MoS₂, JCPDS 37-1492), respectively. For MoS₂/CNFs sample, a new broad peak centered at around 2θ of 22.4° should be the typical characteristic peak of the stacked CNFs.¹⁶ However, the intensity of diffraction peaks of the decorated MoS₂ in CNFs framework significantly decreased. It indicates strongly that the incorporation of CNFs considerably restrains the aggregation of MoS₂ nanoparticles during the solvothermal synthesis process, which is in agreement with previously reported results.^{21,24} Moreover, Raman spectroscopy strongly indicates the presence of MoS₂ on the CNFs. As shown in Figure S3 (b), MoS₂/CNFs composite exhibits the characteristic peaks of MoS₂ and the D and G bands of carbon in the hybrid. As a consequence, the observed small size and poor crystallinity of MoS₂ should be beneficial for HER.

It is known that the valence of Mo in the composite provides important information for understanding the HER activity of the catalysts.³¹ Thus, we investigated the atomic valence states and the composition of the MoS₂/CNFs sample by X-ray photoelectron spectroscopy (XPS). Figure 3a confirms the elemental composition of MoS₂/CNFs with the peaks of Mo, S, C and O. Figure 3b presents the high-resolution XPS spectra, showing that the C 1s core level can be deconvoluted into two peaks. The main peak at 284.4 eV is assigned to sp² hybridized graphite-like carbon atom and the peak around 285.9 eV is attributed to carbon atom bound to one oxygen atom. The C 1s peaks are in consistent with the reported data for CNFs.²⁶ On the other hand, the high-resolution XPS of Mo 3d region is shown in Figure 3c, which can be deconvoluted into five peaks. One peak at 226.2 eV is actually assigned to S 2s. The other two main intense peaks at 228.6 eV and 231.9 eV are characteristic signals of Mo 3d_{5/2} and Mo 3d_{3/2}, respectively. Further, we observed a binding energy peak at 235.4 eV (Mo^{VI}). It should be assigned to MoO₃ or MoO₄²⁻, which might be resulted from the oxidation of the sample in air.³²⁻³³ Also, a shoulder peak at binding energy around 230.1 eV indicates that Mo^{VI} was partially reduced to Mo^V as an intermediate phase. In addition to Mo element, sulfur species were further determined from the high-resolution XPS spectrum of S 2p (Figure 3d). The main doublet located at binding energies of 161.5 and 163.5 eV corresponds to the S 2p_{3/2} and S 2p_{1/2} of MoS₂, respectively. Meanwhile, the binding energy at 164.6 eV suggests the existence of bridging disulfides S₂²⁻ and/or apical S²⁻ ligands, which are believed to closely associated with the high HER activity of the catalyst. The peak of 168.2 eV can be assigned to S^{IV} species in sulfate groups (SO₃²⁻). We noted

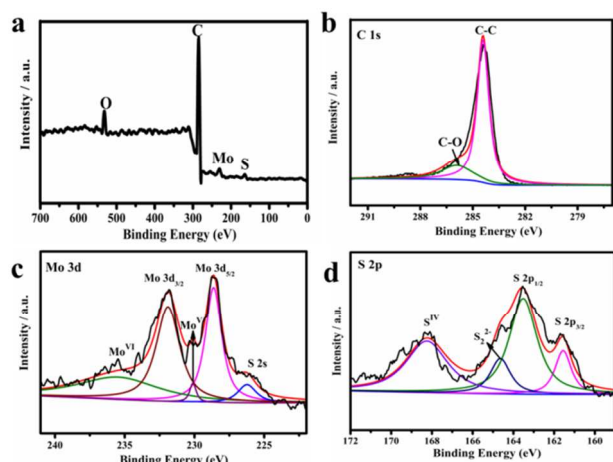


Figure 3. (a) XPS survey spectra and (b–d) high-resolution XPS spectra of MoS₂/CNFs composites.

5 that these groups could locate at edges of MoS₂ layers, which were still present even after washing with soluble salts. Finally, the analysis of the Mo (3d) and S (2p) peak intensities yields an S/Mo atomic ratio of 2.19–2.29. In addition, we calculate the mass of MoS₂ on CNFs by thermogravimetric analysis (TGA).
 10 We measured TG curves of the MoS₂/CNFs, the bare MoS₂ nanoparticles and the bare CNFs under air atmosphere at a heating rate of 10 °C min⁻¹, respectively. As shown in Figure S4, the weight content of the MoS₂ in the hybrid is calculated approximately to be 22 %. Taken together the results of SEM,
 15 TEM, XRD, XPS and TGA presented above, we have demonstrated a novel nanostructured catalyst, which consists of nanosized, low-crystallinity MoS₂ nanoparticles and 3D porous CNFs framework.

Apart from these features, this novel catalyst appears as
 20 bulky electrode with unique elastic properties. Figure S5 shows the images that revealing the compression test for the MoS₂/CNFs foam. The foam can sustain large-strain deformations (~70%) under manual compression and recover most of the material volume without obviously structural fatigue
 25 within 20 s. Such a flexible property should be attributed to both the inherent flexibility of CNFs and the unique interconnected 3D networks of monolithic CNF aerogels. Thus, when using as electrode, it avoids the using of binder, which is mostly required by traditional powder catalyst. Moreover, the excellent structural
 30 mechanical stability enables it as a robust catalyst with a unique 3D architecture, which can be easily used to fabricate various electrochemical devices.

The HER electrocatalytic activity of the MoS₂/CNFs composite was investigated in 0.5 M H₂SO₄ solution using a
 35 typical three-electrode setup. A piece of the foam was used as a bulky electrode with a connected Ag wire as current collector. For control experiment, we also examined the HER performance of commercial Pt catalyst (10 wt % Pt on Vulcan carbon black). The linear sweep voltammetry (LSV) was recorded at
 40 MoS₂/CNFs foam electrode, showing a small overpotential (η) of ~0.12 V for HER (Figure 4a). It shows that the cathodic current increased rapidly along with negative potential scanning. In sharp contrast, free MoS₂ nanoparticles or CNFs alone exhibited very low HER activity, as shown in Figure 4a. Thus, it suggests that

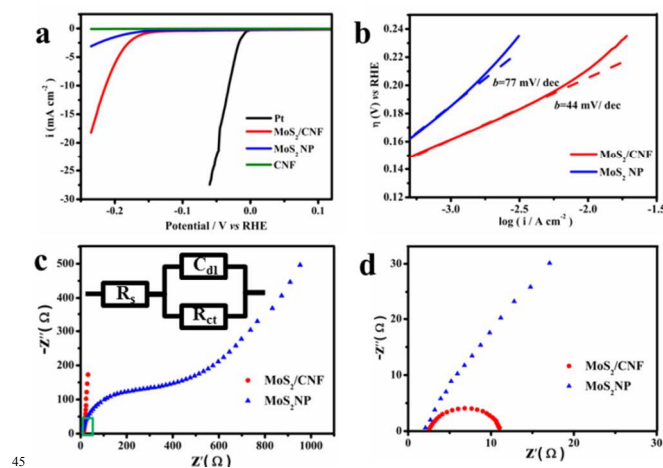


Figure 4. (a) The LSV polarization curves obtained with several catalysts. (b) The Tafel plots of MoS₂ nanoparticles and MoS₂/CNFs nanostructures. (c) The corresponding AC impedance spectroscopy of MoS₂ nanoparticles and MoS₂/CNFs nanostructures. The inset plot is the equivalent electrical circuit
 50 used to model the HER process on the as-prepared MoS₂ catalysts. (d) The enlarge figure of the green rectangle in (c).

the incorporation of MoS₂ into the CNFs foam should greatly enhance HER activity. To clarify the role of CNFs foam, we next
 55 examined the HER performance of the sample that consists of MoS₂ particles and carbon black, which were physically mixed with a similar C: Mo ratio. As shown in Figure S2, this sample exhibits much poorer activity than the as-prepared MoS₂/CNFs foam. Therefore, it suggests that a 3D and porous CNFs
 60 framework is crucial for achieving high performance HER catalysts. The linear portions of the Tafel plots (Figure 4b) were fit to the Tafel equation ($\eta = b \log j + a$, where j is the current density and b is the Tafel slope), yielding Tafel slopes of ~44 and ~77 mV dec⁻¹ for the MoS₂/CNFs foam and pure MoS₂
 65 nanoparticles, respectively. The calculated Tafel value of MoS₂/CNFs is comparable to that of most reported MoS₂-based HER electrocatalysts, which are listed in Supporting Information Table S1 for comparisons. According to classical theory of hydrogen generation, a Tafel slope of around 40 mV dec⁻¹
 70 indicates the rate determining step is the electrochemical desorption of H_{ads} and H₃O⁺ to form hydrogen and the HER occurs through a Volmer-Heyrovsky mechanism at the MoS₂/CNFs foam electrode.

The presence of well-conductive CNFs in the composite
 75 should improve electron transport between the poor conducted MoS₂ nanoparticles and the electrode. To verify this assumption, electrochemical impedance spectra (EIS) was then performed. The Nyquist plots of the samples and the corresponding electrical equivalent circuit diagram are given in Figure 4c. The Figure 4d
 80 is the enlarge figure of the green rectangle in Figure 4c. As shown in Figure 4c and 4d, the MoS₂/CNFs foam electrode gives low charge-transfer impedance (R_{ct}) of ~9 Ω , while the bare MoS₂ electrode shows high R_{ct} of ~450 Ω . The remarkable decrease of R_{ct} for MoS₂/CNFs foam electrode implies faster
 85 HER kinetics, which is believed to contribute significantly to its high HER performance.

On the other hand, the crystalline of MoS₂ also affects the

HER activity.³⁴ To confirm this, a sample was prepared by annealing MoS₂/CNFs at 800 °C. XRD spectra of the annealed sample, as shown in Figure S6, displays sharp peaks with very high intensity in comparison with the MoS₂/CNFs sample before annealing. Especially, the strong (015) peak at $2\theta = 41.7^\circ$ verifies a well-stacked layered structure of MoS₂ in the sample obtained at 800 °C, indicating high crystallinity of MoS₂ after annealing. However, as shown in Figure S7, the sample obtained at 800 °C displays very low HER activity with a much higher Tafel slope of ~155 mV dec⁻¹ than the sample before annealing. This observation is in agreement with the previously reported results.²¹ To further explain the different performance of MoS₂/CNFs foam before and after annealing, we calculate the electrochemical active sites and turnover frequency (TOF).²¹ We attempted to quantify the active sites by measuring the cyclic voltammograms in the region of -0.2 V to 0.6 V vs. RHE. Figure S8 shows the polarization curves normalized by the active sites, and expressed in terms of TOF (see Supporting Information). The TOF per active site for the as-prepared MoS₂/CNFs is calculated to be 0.04 s⁻¹ at $\eta = 0$ mV (vs. 0.0003 s⁻¹ after annealing). Therefore, our modified synthetic method provides a facile and green route to prepare high-performance HER catalyst. The as-prepared MoS₂/CNFs catalyst is supposed to expose much more defect sites or the bridging S₂²⁻ due to the amorphous state of MoS₂ structure. The promising HER activity of the as-prepared MoS₂/CNFs should be ascribed to the low crystalline of MoS₂ obtained with this simple synthetic method.

Apart from the high HER activity, long-term durability is another important parameter of judging the catalyst performance. To evaluate the stability of MoS₂/CNFs in acidic environment, we measured the cyclic voltammetry (CV) of the MoS₂/CNFs foam electrode continuously for 1000 cycles from +0.07 V to -0.43 V vs. RHE at the rate of 5 mV s⁻¹. Figure S9 shows that, after the 1000 cycle's continuous operation, the polarization curve maintains similar shape to the initial one, suggesting high stability of the MoS₂/CNFs electrode for long-term utilization.

In order to further evaluate the HER reactivity, we use the gas chromatography (GC) to detect the gas production at the MoS₂/CNFs electrode. As shown in Figure S10, we only detected H₂ as the product. The amount of collected H₂ shows linear dependence along with the increasing time of HER, which was consistent with the amount of charge passed through the system, indicating essentially 100 % faradaic efficiency for the HER. Moreover, we recorded the movies of the two electrodes of CNF foam and MoS₂/CNFs foam, as shown in the Supporting Information. Vigorous bubble was observed at the MoS₂/CNFs foam electrode along with the positively potential scanning (see Movie S1). In a clear contrast, nearly no bubble was observed even at high potential for the pristine CNFs foam without MoS₂ (see Movie S2). It suggests that the MoS₂/CNFs foam electrode can be directly used as device for electrochemical hydrogen production, which is highly desired for practical application.

4. Conclusions

In summary, we have reported a simple synthetic strategy for the preparation of 3D, flexible and durable MoS₂/CNFs foam electrode for HER. By using CNF hydrogel as a well-conductive and flexible substrate, the decoration of uniformly distributed

MoS₂ nanoparticles on such CNFs framework leads to the formation of 3D and porous HER catalyst. This novel structured HER catalyst exhibits a low overpotential of 120 mV and a small Tafel slope of 44 mV dec⁻¹. Moreover, the MoS₂/CNFs catalyst exhibits promising stability after 1000 cycle's measurement. Remarkably, the easy manipulation and flexible properties of the MoS₂/CNFs foam offer the advantages of binder-free in preparing HER electrode, as well as other functional electrochemical devices. This work paves a viable way for fabricating high efficient and flexible electrode for large-scale water splitting technology.

Notes and references

- a: Beijing Key Laboratory for Chemical Power Source and Green Catalysis, School of Chemical Engineering and Environment, Beijing Institute of Technology, Beijing, 100081, People's Republic of China
 b: National Key Laboratory of Power Sources, Tianjin Institute of Power Sources, Tianjin, 300381, People's Republic of China
 † &: These two authors have the same contribution to this work.
 E-mail: bityanyiming@163.com; bitkeningsun@163.com; liuting@bit.edu.cn; Tel & Fax: 0086-10-68918696.
 ‡ Electronic Supplementary Information (ESI) available: [Figure S1-10, Table S1, Movie S1 and Movie S2]. See DOI: 10.1039/b000000x/
- M. S. Dresselhaus, I. L. Thomas, *Nature*, 2001, **414**, 332-337.
 - B. Rausch, M. D. Symes, G. Chisholm, L. Cronin, *Science*, 2014, **345**, 1326-1330.
 - M. G. Walter, E. L. Warren, J. R. McKone, S.W. Boettcher, Q. Mi, E. A. Santori, N. S. Lewis, *Chem. Rev.*, 2010, **110**, 6446-6473.
 - T. F. Jaramillo, K. P. Jorgensen, J. Bonde, J. H. Nielsen, S. Horch, I. Chorkendorff, *Science*, 2007, **317**, 100-102.
 - Y. Hou, B. Zhang, Z. H. Wen, S. M. Cui, X. R. Guo, Z. He, J. H. Chen, *J. Mater. Chem. A*, 2014, **2**, 13795-13800.
 - Y. H. Chang, F. Y. Wu, T. Y. Chen, C. L. Hsu, C. H. Chen, F. Wiryo, K. H. Wei, C. Y. Chiang, L. J. Li, *Small*, 2014, **10**, 895-900.
 - J. Kibsgaard, Z. Chen, B. N. Reinecke, T. F. Jaramillo, *Nat. Mater.*, 2012, **11**, 963-969.
 - Z. Chen, D. Cummins, B. N. Reinecke, E. Clark, M. K. Sunkara, T. F. Jaramillo, *Nano Lett.*, 2011, **11**, 4168-4175.
 - D. Kong, H. Wang, J. J. Cha, M. Pasta, K. J. Koski, J. Yao, Y. Cui, *Nano Lett.*, 2013, **13**, 1341-1347.
 - H. Tang, K. P. Dou, C. C. Kaun, Q. Kuang, S. H. Yang, *J. Mater. Chem. A*, 2014, **2**, 360-364.
 - W. Chen, C. Wang, K. Sasaki, N. Marinkovic, W. Xu, J. T. Muckerman, Y. Zhu, R. R. Adzic, *Energy Environ. Sci.*, 2013, **6**, 943-951.
 - D. H. Youn, S. Han, J. Y. Kim, J. Y. Kim, H. Park, S. H. Chio, J. S. Lee, *ACS Nano.*, 2014, **8**, 5164-5173.
 - H. Vrubel, X. Hu, *Angew. Chem. Int. Ed.*, 2012, **51**, 12703-12706.
 - W. Chen, K. Sasaki, C. Ma, A. I. Frenkel, N. Marinkovic, J. T. Muckerman, Y. Zhu, R. R. Adzic, *Angew. Chem. Int. Ed.*, 2012, **51**, 6131-6135.
 - B. Cao, G. M. Veith, J. C. Neufeind, R. R. Adzic, P. G. Khalifah, *J. Am. Chem. Soc.*, 2013, **135**, 19186-19192.
 - J. Yang, H. S. Shin, *J. Mater. Chem. A*, 2014, **2**, 5979-5985.
 - J. Bonde, P. G. Moses, T. F. Jaramillo, J. K. Nørskov, I. Chorkendorff, *Faraday Discuss*, 2008, **140**, 219-231.
 - L. Liao, J. Zhu, X. J. Bian, L. N. Zhu, M. D. Scanlon, H. H. Girault, B. H. Liu, *Adv. Funct. Mater.*, 2013, **23**, 5326-5333.

- 19 Y. H. Chang, C. T. Lin, T. Y. Chen, C. L. Hsu, Y. H. Lee, W. J. Zhang, K. H. Wei, L. J. Li, *Adv. Mater.*, 2013, **25**, 756-760.
- 20 C. B. Ma, X. Y. Qi, B. Chen, S. Y. Bao, Z. Y. Yin, X. J. Wu, Z. M. Luo, J. Wei, H. L. Zhang, H. Zhang, *Nanoscale*, 2014, **6**, 5624-5629.
- 5 21 Y. Yan, X. M. Ge, Z. L. Liu, J. Y. Wang, J. M. Lee, X. Wang, *Nanoscale*, 2013, **5**, 7768-7771.
- 22 X. J. Bian, J. Zhu, L. Liao, M. D. Scanlon, P. Y. Ge, C. Ji, H. H. Girault, B. H. Liu, *Electrochem. Commun.*, 2012, **22**, 128-132.
- 23 Y. G. Li, H. L. Wang, L. M. Xie, Y. Y. Liang, G. S. Hong, H. J. Dai, *J. Am. Chem. Soc.*, 2011, **133**, 7296-7299.
- 10 24 X. L. Zheng, J. B. Xu, K. Y. Yan, H. Wang, Z. L. Wang, S. H. Yang, *Chem. Mater.*, 2014, **26**, 2344-2353.
- 25 H. Zhu, M. L. Du, M. Zhang, M. L. Zou, T. T. Yang, Y. Q. Fu, J. M. Yao, *J. Mater. Chem. A*, 2014, **2**, 7680-7685.
- 15 26 Z. Y. Wu, C. Li, H. W. Liang, J. F. Chen, S. H. Yu, *Angew. Chem. Int. Ed.*, 2013, **52**, 2925-2929.
- 27 L. F. Chen, Z. H. Huang, H. W. Liang, W. T. Yao, Z. Y. Yu, S. H. Yu, *Energy Environ. Sci.*, 2013, **6**, 3331-3338.
- 28 L. F. Chen, Z. H. Huang, H. W. Liang, H. L. Gao, S. H. Yu, *Adv. Funct. Mater.*, 2014, **24**, 5104-5111.
- 20 29 L. F. Chen, Z. H. Huang, H. W. Liang, Q. F. Guan, S. H. Yu, *Adv. Mater.*, 2013, **25**, 4746-4752.
- 30 F. Zhou, S. Xin, H. W. Liang, L. T. Song, S. H. Yu, *Angew. Chem. Int. Ed.*, 2014, **53**, 11552-11556.
- 25 31 Y. Yan, B. Y. Xia, Z. C. Xu, X. Wang, *ACS. Catal.*, 2014, **4**, 1693-1705.
- 32 V. O. Koroteev, L. G. Bulusheva, I. P. Asanov, E. V. Shlyakhova, D. V. Vyalikh, A. V. Okotrub, *J. Phys. Chem. C*, 2011, **115**, 21199-21204.
- 30 33 H. W. Wang, P. Skeldon, G. E. Thompson, *Surf. Coat. Technol.*, 1997, **91**, 200-207.
- 34 H. Vrabel, D. Merki, X. Hu, *Energy Environ. Sci.*, 2012, **5**, 6136-6144.